Robert C. Smith, MD • Robert C. Lange, PhD • Shirley M. McCarthy, PhD, MD

Chemical Shift Artifact: Dependence on Shape and Orientation of the Lipid-Water Interface[1]

On magnetic resonance images, chemical shift artifact (CSA) can be seen at a planar lipid-water interface oriented within the plane of the phase-encoding and section-select directions (ie, perpendicular to the frequency-encoding direction). Phantoms and a clinical case were used to demonstrate that when a lipid-water interface is curvilinear (eg, spherical) or planar but not oriented along the section-select direction, CSA may be absent or diminished. This effect can be seen at interfaces of normal structures (kidneys, bladder) as well as at interfaces with pathologic lesions such as lipid-containing dermoids. Not only is this effect dependent on section thickness, field of view, matrix size, and receiver bandwidth, but it is also strongly dependent on the orientation of the interface with respect to the section-select direction. Knowledge of the factors that can alter CSA is important since it is used to distinguish lipid-containing from nonlipid-containing structures of similar signal intensities.

Index terms: Dermoid, 852.313 • Endometriosis, 85.3192 • Magnetic resonance (MR), artifact • Magnetic resonance (MR), chemical shift • Magnetic resonance (MR), experimental • Pelvis, MR studies, 85.1214, 852.313, 85.3192

Radiology 1991; 181:225–229

CHEMICAL shift artifact (CSA) and the potential pitfall of labeling it as a disease process have been described previously (1–3). The presence of this artifact within or contiguous to a lesion is, nonetheless, a key observation enabling the diagnosis of a lipid-water interface. In magnetic resonance (MR) imaging of the female pelvis, CSA is particularly useful in differentiating a dermoid from an endometrioma. The former diagnosis necessitates surgery, whereas the latter may be treated conservatively.

On MR images obtained from women with adnexal masses, we noticed that surgically proved dermoids did not always exhibit CSA. Similarly, we noted that at the lipid-water interface of normal structures (eg, kidneys surrounded by perirenal fat, bladder surrounded by perivesical fat), CSA is not always apparent. We undertook this study to examine why CSA is present at some lipid-water interfaces and absent or diminished at others.

MATERIALS AND METHODS

Initially, images of phantoms were obtained. A solution consisting of liquid oil in water was used to create a planar lipid-water interface. The oil layered on the water, creating an interface within the coronal plane. The water was titrated with copper chloride so that the ratio of signal intensities of the oil and water on T1-weighted spin-echo (SE) 500/20 (repetition time [TR] msec/echo time [TE] msec) images was 2.5—approximately the same as that of subcutaneous fat and soft tissue within the body. Spheres of solid vegetable shortening embedded in gelatin were used to create a spherical lipid-water interface. The spheres varied in diameter from 1.5 to 3.5 cm.

Imaging was conducted within a linear transmit-and-receive extremity coil with use of a 1.5-T system (Signa; GE Medical Systems, Milwaukee). A 256 × 256 matrix with two excitations per phase-encoding step was used to minimize Gibbs artifact and produce an adequate signal-to-noise ratio. The majority of the images were obtained with a TR of 500 msec, a TE of 20 msec, and a 28-cm field of view (FOV)—a size comparable to that typically used for pelvic MR imaging. FOVs of 8 and 48 cm (the allowable instrument extremes) were also used to demonstrate the effect of this parameter on CSA. Section thicknesses included were 3, 5, 7, and 10 mm. The standard receiver bandwidth of ±16 kHz was used for all images. Identical transmit-and-receive gain settings were used for images of equal section thickness and FOV.

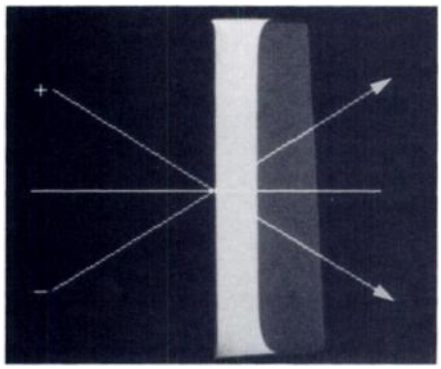

Figure 1. The convention for the sign of the angle of obliquity.

For the planar interface of the oil-water phantom, a sagittal localizer image was obtained and used to prescribe oblique axial sections. The angle of obliquity could be varied in 1° increments by using the graphic prescription feature of the imager. The angle was defined with respect to an axis oriented perpendicular to the interface (ie, the standard axial plane of section). The angle was denoted as positive or negative with the convention shown in Figure 1 and could be oriented in the direction of either increasing or decreasing frequency with respect to the direction of the section-select gradient. The frequency-encoding direction (FED) is along the line of the graphical prescription, with the direction of increasing frequency as indicated in Figure 1.

Abbreviations: CSA = chemical shift artifact, FED = frequency-encoding direction, FOV = field of view, SE = spin echo, TE = echo time, TR = repetition time.

[1] From the Department of Diagnostic Imaging, Yale School of Medicine, 333 Cedar St, New Haven, CT 06510. Received April 5, 1991; revision requested May 14; revision received and accepted May 28. **Address reprint requests to** R.C.S.

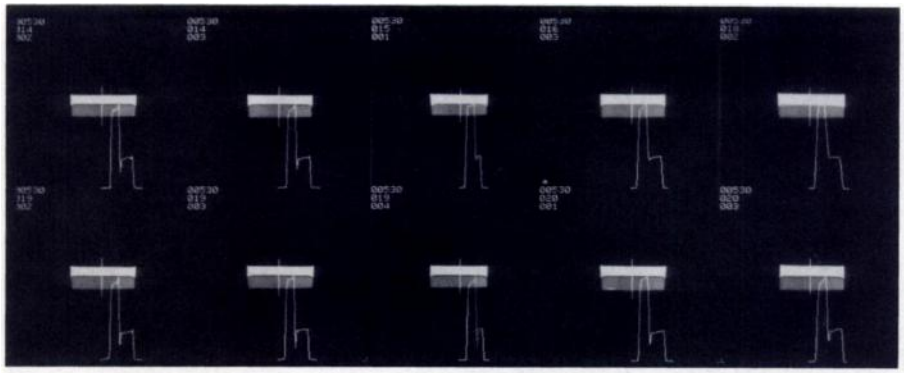

Figure 2. Axial oblique images with section thickness of 10 mm and FOV of 28 cm. Top row, from left to right: −5°, −10°, −15°, −20°, −30°. Bottom row, from left to right: +5°, +10°, +15°, +20°, +30°. For this section thickness, the CSA disappears at $\theta \leq -20°$ but remains apparent for $0° < \theta \leq 30°$.

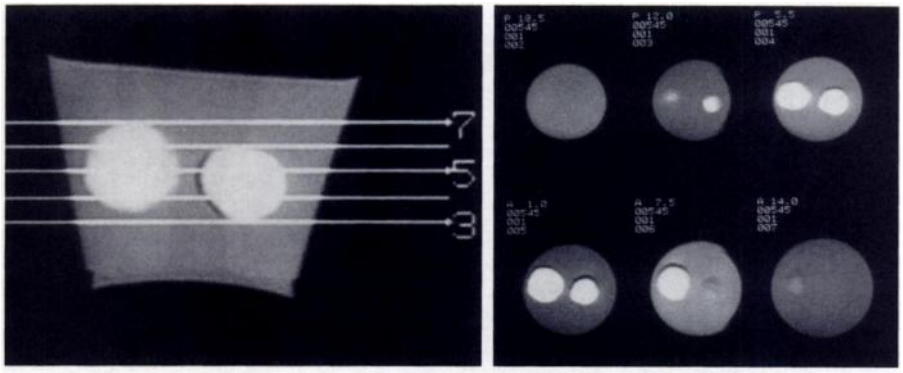

a. **b.**

Figure 3. **(a)** Axial localizer image of lipid spheres in gelatin. The numbers on the right correspond to image number. **(b)** Depiction of 5-mm-thick coronal images as indicated on localizer image. Fourth row of numbers indicates image number. The CSA is apparent in image 5 (bottom row, left), which was obtained through the center of the sphere. On image 4 (top row, right), which is located on the low-frequency side of the section-select gradient with respect to the center of the sphere, CSA is almost completely absent. On image 6 (bottom row, middle), which is located on the high-frequency side of the section-select gradient, CSA is readily apparent.

Figure 4. Sagittal image obtained through the center of a dermoid. CSA is readily apparent on both inferior and superior surfaces that are relatively flat.

Table 1
Critical Angle for FOV of 28 cm

Section Thickness (mm)	Critical Angle
10	$\leq -19°$
7	$\leq -22°$
5	$\leq -29°$
3	$\leq -36°$

Note.—The critical angle is that at which the CSA is no longer apparent.

Table 2
Negative Critical Angles as a Function of FOV

FOV (cm)	Critical Angle
8	$\leq -6°$
16	$\leq -10°$
28	$\leq -19°$
48	$\leq -36°$

Note.—Only negative angles were tested with varying FOV. Section thickness = 10 mm.

The oblique axial images of the lipid-water phantom were evaluated for the presence or absence of CSA at the lipid-water interface. This evaluation was made visually as well as by profile analysis. The profile analysis displays a plot of signal intensity as a function of position (with 1-pixel position increments) along a line perpendicular to the interface. Multiplanar images obtained through the lipid spheres were evaluated visually for presence or absence of CSA.

A clinical study was also used to verify observations. The patient, a 42-year-old woman, was referred for MR imaging to evaluate an adnexal mass visualized at ultrasound but indeterminate for type of disease process. Subsequent pathologic examination of the mass showed it to be a dermoid, consisting almost entirely of lipid. The patient was imaged in the body coil with use of respiratory compensation, saturation pulses, no phase wrap, and glucagon. The respiratory compensation option reorders the phase-encoding steps based on respiratory motion to reduce phase artifacts from structures with periodic motion. Saturation pulses applied outside the imaging volume reduce vascular pulsation artifacts. Parameters consisted of axial T1-weighted (SE 500/20) images, with 5- and 10-mm section thicknesses, 2.5-mm intersection spacing, 28-cm FOV, 256 × 128 matrix, and two excitations. Axial and sagittal intermediate and T2-weighted (SE 1,700/20–80) images were obtained with 5-mm-thick sections, 2.5-mm intersection spacing, 28-cm FOV, 256 × 128 matrix, and two excitations.

RESULTS

With the acquisition of oblique axial sections through the planar lipid-water interface, the angle of obliquity θ at which CSA became absent was found to depend on section thickness, FOV, and orientation of the plane of section (ie, positive or negative angulation).

Images obtained with a 28-cm FOV, 10-mm section thickness, and positive and negative angles of obliquity are shown in Figure 2. Each image includes a signal intensity profile. The profile is a plot of signal intensity as a function of position along the line shown in the image. The profile analysis was used to avoid Mach effect errors inherent in direct visual inspection of images with sharp interfaces.

With a 10-mm section thickness, CSA gradually diminished as θ was varied in 5° increments with negative angulation. CSA is absent for $\theta = -20°$ or greater negative angulation

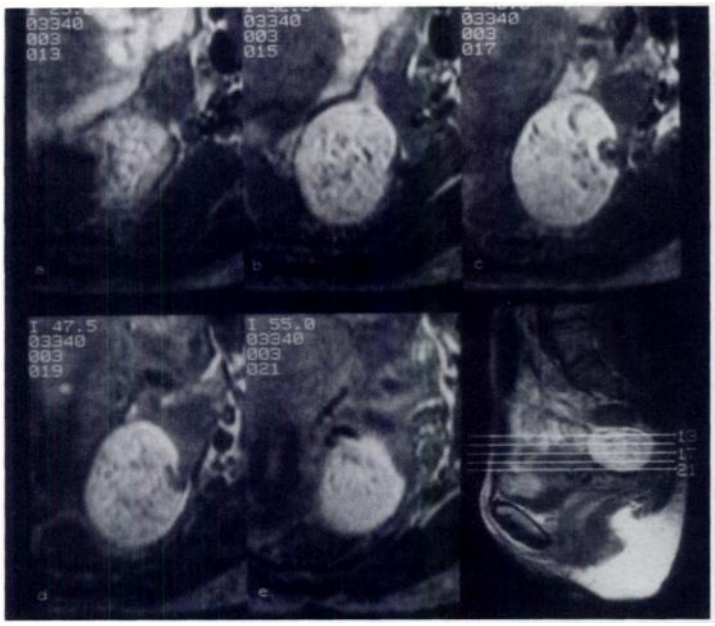

5.

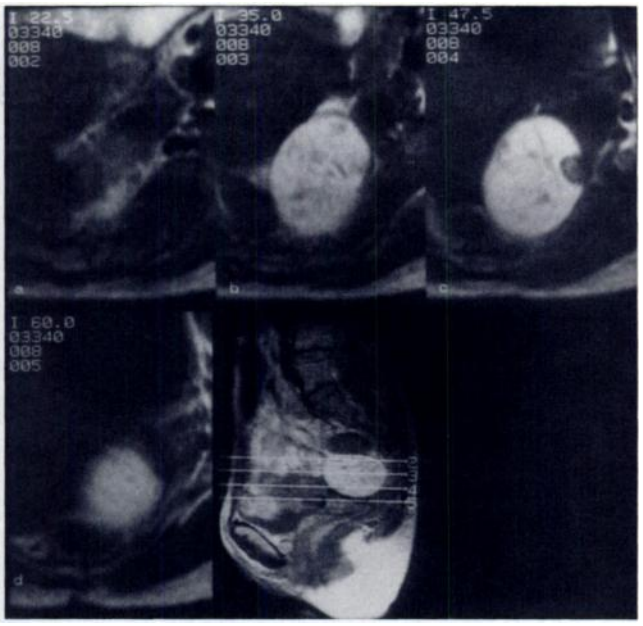

6.

Figures 5, 6. Bottom row of numbers indicates image number. **(5)** Adjacent 5-mm-thick axial views (*a–e*) obtained through a dermoid in planes indicated on sagittal localizer image (bottom right). CSA is readily apparent on image 15 (*b*) obtained at the high-frequency side of the section-select gradient. CSA is less visible on images 19 (*d*) and 21 (*e*), which are from the low-frequency side. Note correspondence with images in Figure 3. **(6)** Adjacent 10-mm-thick axial views (*a–d*) obtained through a dermoid in planes indicated on sagittal localizer image. CSA is essentially absent in all sections.

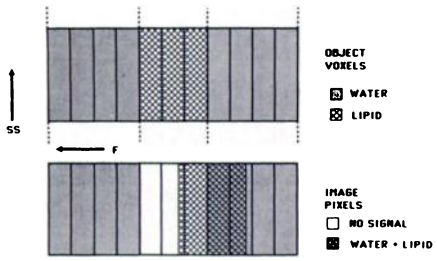

Figure 7. Top: Representation of a row of object voxels viewed perpendicular to the section-select direction. Arrows indicate the section-select gradient direction (*SS*) and FED (*F*) from low to high frequency. Bottom: The well-known chemical shift misregistration, due to the lower resonance frequency of lipid protons, is depicted.

(Fig 2). As θ was varied in 5° increments with positive angulation, CSA remained apparent at θ = +30° (Fig 2) and was present to θ = +45°, the largest positive angle tested (not shown).

As section thickness was decreased through 7, 5, and 3 mm with a 28-cm FOV, the negative angle of obliquity at which CSA was absent (the critical angle) increased in magnitude. The critical angles are shown in Table 1. For positive angles of obliquity (up to the maximum tested of +45°), CSA remained apparent for these section thicknesses.

Images were also obtained with a 10-mm section thickness and varying FOV. The negative critical angles for various FOVs are given in Table 2. The magnitude of the negative critical angle increases with increasing FOV.

These results demonstrate a dependence on section thickness, FOV, and orientation of the plane of section. The appearance of CSA is clearly not symmetric about zero obliquity (ie, with all other parameters identical, the appearances of CSA on sections obtained at +θ° and −θ° are not equivalent).

The images obtained through lipid spheres embedded in gelatin are shown in Figure 3. These are adjacent images obtained through two lipid spheres. The appearance of CSA can be seen to depend on the location of the section with respect to the section-select gradient direction. CSA is less apparent when the section is located in that half of the sphere on the low-frequency side of the section-select direction (Fig 3).

Images obtained through a pathologically proved dermoid consisting almost entirely of lipid are shown in Figures 4–6. The superior and inferior surfaces of the dermoid are relatively flat so that CSA is readily seen along these surfaces on sagittal images. Images obtained with axial 5- and 10-mm-thick sections demonstrate the dependence of the appearance of CSA on section thickness and location. With 5-mm-thick sections, CSA is readily seen through the center of the dermoid and on the high-frequency side of the section-select gradient direction (cf Fig 3). With 10-mm-thick sections, CSA is not visible.

DISCUSSION

The theoretical basis of the results described depends on two effects. The first is chemical shift misregistration along the FED. This effect is well known. The second is chemical shift misexcitation along the section-select direction. The effect of misexcitation has not been previously described in clinical imaging, but is a known effect (4).

To review the first effect, at a field strength of 1.5 T, the precession frequency of water protons is approximately 220 Hz greater than that of lipid protons. This causes misregistration of the position of lipid proton voxels along the FED with a positional shift toward the direction of decreasing frequencies.[2] At a planar lipid-water interface oriented perpendicular to the FED, this positional misregistration can cause two effects: A

[2] When the field strength is G (in tesla), the bandwidth along the FED is ΔB_t, and the number of frequency encodings is N_t, the location of lipid protons will be shifted $(220/1.5) \cdot G \cdot (N_t/\Delta B_t)$ pixels in the direction of decreasing frequency. On the Signa system, G = 1.5 T and $\Delta B_t = 3.2 \times 10^5$ Hz. When 256 frequency encodings are used, this shift will equal 1.76 pixels.

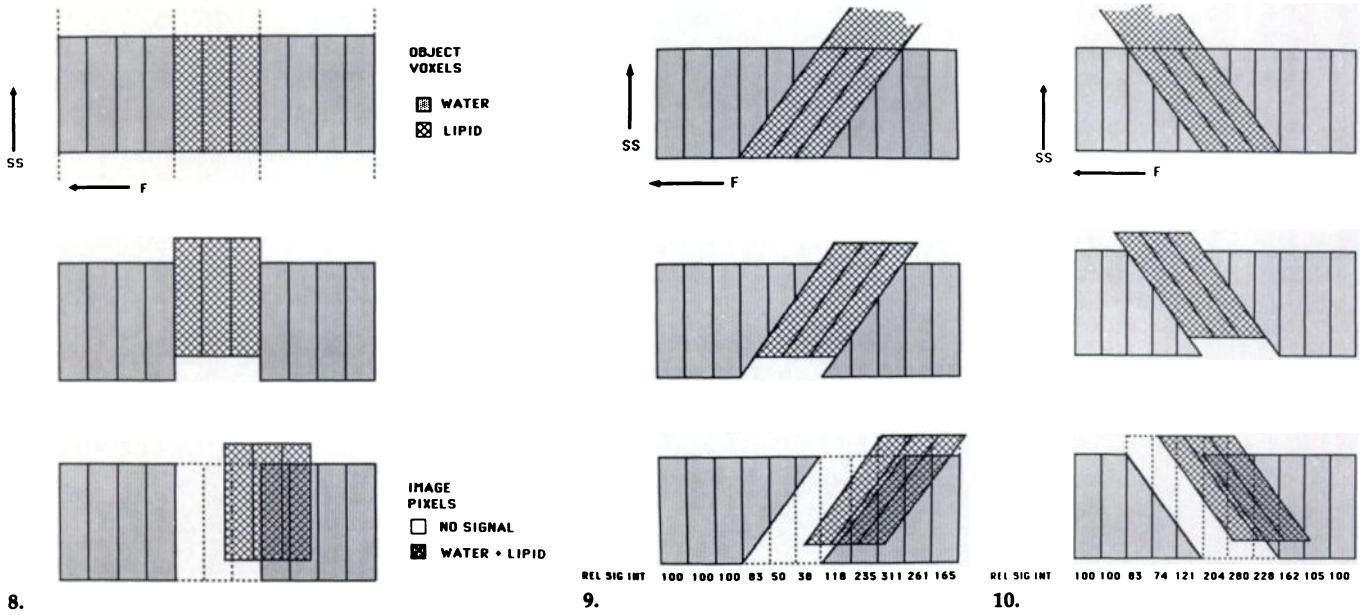

8. 9. 10.

Figures 8–10. Arrows indicate the section-select gradient direction (*SS*) and FED (*F*) from low to high frequency. **(8)** Top: Representation of a row of object voxels viewed perpendicular to the section-select direction. Middle: Chemical shift misexcitation. The low-frequency side of the section-select gradient is on the inferior side of the row of voxels. Bottom: The result of chemical shift misexcitation combined with chemical shift misregistration. **(9)** Top: A model of a lipid object with parallel sides in water, oriented obliquely to both section-select and frequency-encoding gradients. Middle: Chemical shift misexcitation. Bottom: The combination of chemical shift misexcitation and chemical shift misregistration. The numbers below the image pixels are relative signal intensities assuming a 37° angle of obliquity, 5-mm section thickness, 32-cm FOV, 256 frequency encodings, and a bandwidth of ±16 kHz. Signal intensity of lipid is equal to 2.5 times that of water. There is a sharp drop in signal intensity at the water-lipid interface and a bright strip at the lipid-water interface. **(10)** Top: A model of a lipid object with parallel sides in water, with orientation opposite of that in **9.** Middle: Chemical shift misexcitation. Bottom: Combination of misexcitation and misregistration, with same imaging parameters and relative signal intensities as in **9.** There is only a small decrease in signal intensity at the water-lipid interface. The bright strip at the lipid-water interface remains.

linear band of pixels with decreased signal intensity occurs at the interface when lipid is on the low-frequency side of the FED (with respect to water). This results from the lipid pixels being shifted *away* from the water pixels, which leaves pixels on the lipid side of the interface with absent signal. A linear band of pixels with increased signal intensity occurs at the interface when lipid is on the high-frequency side of the FED (with respect to water). This results from the lipid pixels being shifted *toward* the water pixels, which causes pixels on the water side of the interface to have signal intensity equal to the sum of the lipid- and water-containing pixels. This effect is illustrated in Figure 7.

A similar effect will occur along the section-select direction due to the difference in precessional frequencies of lipid and water protons. When resonance frequency excitation pulse is applied to a lipid-containing region in the presence of the section-select gradient, the actual region of lipid excited will be shifted along the section-select direction causing a misexcitation. A linear band of lipid within the region on the low-frequency side of the section-select gradient will remain unexcited. Similarly, when lipid is present beyond the section to be excited, a linear band of lipid at the high-frequency side of the section-select gradient will be excited and contribute to the received signal.[3] This effect is illustrated in Figure 8.

At a planar lipid-water interface not oriented along the section-select di-

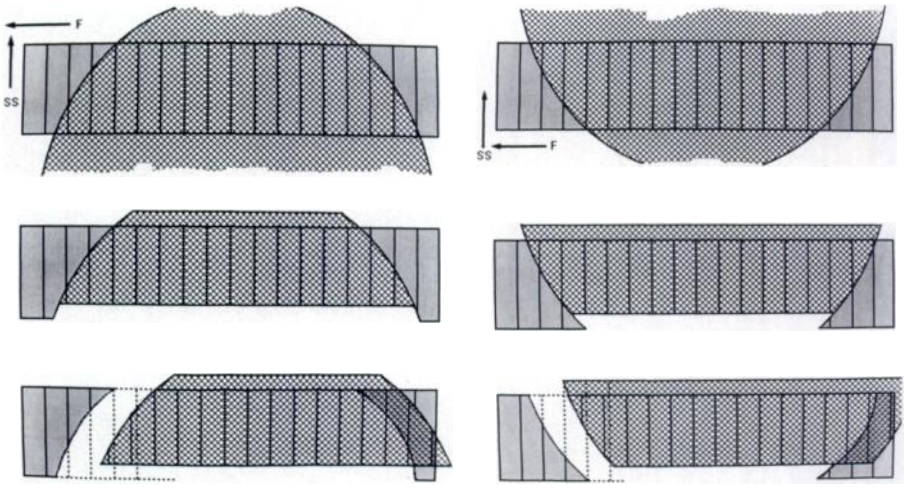

11. 12.

Figures 11, 12. Arrows indicate the section-select gradient direction (*SS*) and FED (*F*) from low to high frequency. **(11)** Top: A model of a spherical lipid object in water. Middle: Chemical shift misexcitation. Bottom: The misexcitation and misregistration produces a sharp drop in signal intensity at the water-lipid interface. **(12)** Top: Model of a lipid sphere in water. Middle: Chemical shift misexcitation. Bottom: The misexcitation and misregistration produces only a modest decrease in signal intensity at the lipid-water interface.

[3] When the resonance frequency excitation bandwidth along the section-select direction is ΔB_r, field strength is G (tesla), and the thickness of the section is ΔT, the misexcitation will extend over a length $(220/1.5) \cdot G \cdot (\Delta T/\Delta B_r)$ along the section-select direction. For standard images on the Signa system, ΔB_r = 1276 Hz and G = 1.5 T.

rection (and therefore also not perpendicular to the FED), voxels along the interface contain both lipid and water protons. Therefore, when the lipid-containing region is on the low-frequency side of the FED, positional misregistration of the lipid proton voxels no longer results in pixels with absent signal. Similarly, when lipid is on the high-frequency side of the FED, positional misregistration of lipid proton voxels no longer results in pixels with signal intensity equal to the sum of a water pixel and a lipid pixel. This effect is dependent on the number of pixels along which the interface extends.[4] In addition, due to chemical shift misexcitation along the section-select direction, the above effect is also dependent on the sign of the angle θ as defined in Figure 1. These effects are illustrated in Figures 9 and 10.

At a spherical lipid-water interface, the effect of positional misregistration along the FED will be similar to that described previously. The effect of chemical shift misexcitation will depend on whether the section is within that half of the spherical interface on the low- or high-frequency side of the section-select direction.[5] These effects are shown in Figures 11 and 12. The number of pixels along which the interface extends will depend on the radius of curvature of the sphere.[4]

A common application of these effects in the female pelvis is in the differential diagnosis of an ovarian mass—specifically, in distinguishing between an endometrioma and a dermoid. Depending on the age of the blood, endometriomas can have signal intensity characteristics that are identical to those of dermoids (on conventional T1- and T2-weighted images as well as on short inversion time inversion-recovery images). The presence of CSA within the lesion or at the lesion interface with surrounding tissue is definitive for a dermoid (5). Therefore, knowledge of the parameters that can enhance (or diminish) the appearance of CSA is crucial. Dermoids need surgical removal but do not require urgent or immediate excision as do malignant masses. Endometriomas, the main entity that can be mistaken for a dermoid, do not require surgery, and are often treated with conservative medical therapy (6).

The effect of matrix size and bandwidth on the appearance of CSA was not examined. A decrease in matrix size is equivalent to an increase in FOV. The effect of bandwidth has been previously described (7).

In conclusion, the presence of CSA is an important observation in the differential diagnosis of a lipid-containing mass. One must be aware that, depending on the choice of imaging parameters, plane of section, shape and orientation of the lipid-water interface, and the specific instrument and field strength employed, CSA may be absent even around lipid-containing masses. Manipulation of these parameters may then be necessary to bring out the CSA. In cases in which the findings are not definitive, lipid- or water-suppression techniques should be employed to resolve the question (Kier et al, unpublished data, 1991). ■

Acknowledgment: We thank Robin Greene, RT, for her enthusiastic help.

References

1. Weinreb J, Brateman L, Babcock E, Maravilla K, Cohen J, Horner S. Chemical shift artifact in clinical magnetic resonance images at 0.35 T. AJR 1985; 145:183–185.
2. Soila K, Viamonte M, Piotr S. Chemical shift misregistration effect in magnetic resonance imaging. Radiology 1984; 153:819–820.
3. Haughton V, Prost R. Pituitary fossa: chemical effect in MR imaging. Radiology 1986; 158:461–462.
4. Maler J, Wehrli FW, Field SA, Steen P, Vaurek R, Belt K. Signa users' newsletter (SUN), vol IV no. 3, May 1988.
5. Togashi K, Nishimura K, Itoh H, et al. Ovarian cystic teratomas: MR imaging. Radiology 1987; 162:669–673.
6. Zawin M, McCarthy S, Scoutt L, et al. Monitoring therapy with a gonadotropin-releasing hormone analog: utility of MR imaging. Radiology 1990; 175:503–506.
7. Smith AS, Weinstein MA, Hurst GC, Defremer DR, Cole RA, Duchesneau PM. Intracranial chemical-shift artifacts on MR images of the brain: observations and relation to sampling bandwidth. AJR 1990; 154:1275–1283.

---

[4] If the interface is oriented along the axis of the phase-encoding direction and at an angle θ with respect to the axis of the section-select direction, the interface will extend over P pixels, where $P = \Delta T \cdot \tan\theta \cdot (N_t/\mathrm{FOV})$. For a sphere of radius r, $P = (\Delta T)\, N_t/(r \cdot \mathrm{FOV})$.

[5] On the Signa system, the low-frequency side of the section-select gradient for axial sections is inferior and for coronal sections is posterior.